TECHNISCHE MECHANIK
an open access journal

journal homepage: www.ovgu.de/techmech

Tech. Mech., Vol. 44, Is. 2, (2024), 74–81

Received: 08.07.2024
Accepted: 29.07.2024
Available online: 29.07.2024

An elastohydrodynamic lubrication framework for hip prostheses based on isogeometric analysis

Yan Tong[1] and Michael Müller[1]*

[1] Technische Universität Braunschweig, Institute for Acoustics and Dynamics, Langer Kamp 19, 38106 Braunschweig, Germany

Abstract: The hip prosthesis modeling involves complex fluid-structure interaction between lubricant flow and solid deformation, which is a typical elastohydrodynamic lubrication regime. This study introduces a novel numerical framework for addressing such challenges through Non-Uniform Rational B-Splines (NURBS)-based isogeometric analysis (IGA). A new form of the Reynolds equation, derived in the parametric space of curved surfaces rather than spherical coordinates, is introduced to streamline discretization within the IGA framework and integration with solid mechanics. Additionally, the momentum balance equation is utilized for calculating solid deformations, providing a more accurate description than the conventional Boussinesq approximation. Furthermore, a developed mass-conserving cavitation formulation is incorporated to depict the formation and volumetric distribution of cavitation bubbles in hip prostheses. These equations are discretized utilizing NURBS basis functions and solved simultaneously via the Newton-Raphson method, enabling efficient strong coupling and rapid convergence. This IGA-based framework also facilitates future integration of nonlinear solid deformation and frictional contact.

Keywords: NURBS, Fluid-Structure-Interaction, Reynolds Equation, Cavitation, Biotribology

1 Introduction

The hip joint, one of the largest joints in the human body, plays a crucial role in supporting weight and facilitating dynamic loading. Structurally, it is a ball and socket synovial joint, constituted by the articulation between the pelvic acetabulum and the femoral head. Various factors such as aging, diseases (e.g. rheumatoid arthritis), and trauma can lead to hip joint malfunction, substantially impacting an individual's daily life. Hip replacement surgery, recognized as one of the most successful and effective interventions, offers significant pain relief by substituting the damaged hip joint with a prosthesis. Typically, the prosthesis consists of an acetabular cup and a femoral head (refer to Fig. 1), which serve as functional substitutes for the damaged pelvic acetabulum and femoral head, respectively.

Statistical results from Evans et al. (2019) indicate that artificial hip joints typically possess a lifespan of 15-20 years. However, this duration cannot meet the needs of younger patients or those enthusiastic about physical activities. Consequently, enhancing the design of artificial hip joint systems and extending their lifespan remains a critical research focus. From a tribological perspective, a key factor affecting the lifespan of artificial hip joints is the friction and wear on their surfaces arising from insufficient lubrication. To comprehensively analyze the elastohydrodynamic lubrication regime of artificial hip joints and to improve their design parameters (such as the radial clearance between the femoral head and the acetabular cup, see Walker and Gold (1971)), it is essential to develop a numerical model that accurately describes the pressure buildup within the fluid film and the consequent deformation of the solid surfaces.

Most existing numerical models for hip prostheses are developed within the finite difference method (FDM) framework (e.g., Jin and Dowson (1999), Jagatia and Jin (2001), Wang and Jin (2005), and Askari and Andersen (2019)). They utilize the Reynolds equation in spherical coordinates to describe the flow of synovial fluid between the acetabular cup and the femoral head. The gap height distribution between the solid surfaces is estimated using the initial clearance and the eccentricity of the femoral head. Additionally, these models employ the Boussinesq approximation (refer to Popov (2010) for further details) to calculate the deformation on contact surfaces. This approach is based on half-space theory, which presupposes an infinitely long surface. As a result, its accuracy for modeling deformations on spherical surfaces is inherently limited. Furthermore, the coupling between solid and fluid parts is achieved through the so-called weak coupling. Herein, the discretized Reynolds equation is iteratively solved to compute the pressure distribution for the current gap height distribution, which is then input into the Boussinesq equation to calculate surface deformation and a new gap height distribution. This process is repeated until the solutions converge for both parts, which requires numerous iterations and is highly inefficient.

Notably, cavitation bubbles may appear within the lubricant film when the fluid pressure falls below a certain threshold. These bubbles can either be introduced externally or result from the release of dissolved gases. The gap in the cavitation region is only partially filled with lubricant, and the pressure remains constant. However, the aforementioned models from Jin and Dowson (1999), Jagatia and Jin (2001), Wang and Jin (2005), and Askari and Andersen (2019) do not account for the volume distribution of bubbles within the lubricant film. Instead, they use the Swift-Stieber boundary condition (enforcing pressure gradient at the cavitation interface to be zero, refer to Bhushan (2013)) to describe the pressure rupture caused by cavitation bubbles. Meng et al. (2015) adopt the mass-conserving Jakobsson-Floberg-Olsson (JFO) boundary condition to accurately describe the cavitation

* E-mail address: mi.mueller@tu-bs.de
doi: 10.24352/UB.OVGU-2024-056

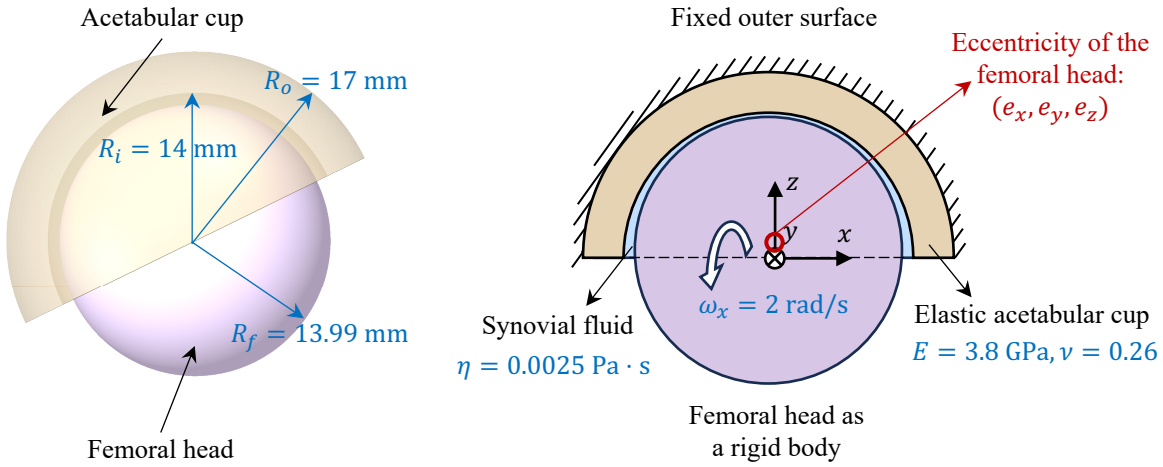

Fig. 1: Schematic diagram of the hip prosthesis: a three-dimensional illustration of the acetabular cup and the femoral head in the hip prosthesis (left); the ball-in-socket configuration for the lubrication analysis in this work (right)

phenomena, but it is still developed based on FDM and weak coupling. The complementarity problem introduced by the JFO boundary condition only makes the convergence process more challenging.

Over recent decades, isogeometric analysis (IGA) proposed by Hughes et al. (2005) has been widely applied in fields such as contact mechanics and fluid dynamics. It can be regarded as a variant of the traditional finite element analysis (FEA), with its core principle involving the use of NURBS (Non-Uniform Rational B-Splines) for both geometry construction and physical field solutions. Thanks to the excellent numerical characteristics of NURBS basis functions, such as high smoothness, IGA is particularly suited for computational mechanics analysis and multiphysics coupling in complex geometric domains.

Our research group (see Müller et al. (2017) and Müller et al. (2018)) focuses on lubricated contact between rough surfaces. Recently, we (Tong et al. (2022)) developed a cavitation formulation within the IGA framework capable of efficiently solving the complementarity problem. This paper will introduce the Reynolds equation defined in the parametric space of a curved surface and combine it with this cavitation formulation to model the lubrication regime in the hip prosthesis. Furthermore, the momentum balance equation governing solid deformation will also be discretized within the IGA framework. The equations for the solid and fluid parts will be solved simultaneously, i.e., strong coupling, with convergence achieved in just a few iterations.

2 Numerical Model

The geometric parameters of the investigated hip prosthesis are derived from Meng et al. (2015), with its three-dimensional construction displayed on the left side of Fig. 1. The acetabular cup has an outer radius of $R_o = 17\,\text{mm}$ and an inner radius of $R_i = 14\,\text{mm}$. The radius of the femoral head is chosen as $R_f = 13.99\,\text{mm}$ such that the initial clearance between the contact surfaces is $c = R_i - R_f = 10\,\mu\text{m}$.

Instead of analyzing the complete hip prosthesis structure, this work utilizes a simplified ball-in-socket configuration to facilitate comparative calculations with Jin and Dowson (1999)'s model based on FDM. Herein, the femoral head is modeled as a rigid sphere, and the acetabular cup is treated as an elastic body with material properties assigned as $E = 3.8\,\text{GPa}$ and $\nu = 0.26$. The external surface of the acetabular cup is fixed, whereas the femoral head oscillates back and forth around the x-axis with an amplitude of $\omega = 2\,\text{rad}\,\text{s}^{-1}$. Nevertheless, this paper does not consider the transient effects induced by the oscillation of the femoral head, but only focuses on the instance of maximum angular velocity for simplicity. When an external force is applied to the femoral head, it undergoes eccentric movement (e_x, e_y, e_z), generating a pressure distribution within the synovial fluid to counteract the applied force. The fluid pressure induces deformation of the acetabular cup, altering the film thickness and, consequently, the pressure distribution itself. This fluid-structure interaction leads to a balanced result between fluid pressure and solid deformation.

As mentioned in Section 1, most existing models on hip prosthesis apply the Reynolds equation in spherical coordinates $(R,\ \theta,\ \phi)$ to describe the lubricant flow. This approach essentially converts the curved surface in Eulerian coordinates into a $(\theta,\ \phi)$ plane through coordinate transformation. The Reynolds equation is then derived on this plane by neglecting the flow in the radial direction (see Jin and Dowson (1999)). However, integrating this equation into the IGA framework presents challenges due to the definition of NURBS basis functions within a distinct parametric space (the knot space, refer to Hughes et al. (2005)). A transformation from spherical to knot coordinates is thus necessary. Moreover, additional coordinate transformations are needed to couple fluid pressure with solid deformation, significantly increasing computational efforts. Therefore, this section will introduce the Reynolds equation derived directly in the parametric space of a curved surface to circumvent these cumbersome transformations.

In the following, the acetabular cup's inner surface and the femoral head's outer surface will be denoted as Γ_2 and Γ_1, respectively (see Fig. 2). Given the minimal clearance between these two surfaces, the fluid flow in the film thickness direction is negligible according to the assumptions of the Reynolds equation (see Bhushan (2013)). Consequently, the fluid velocity is considered tangential to the curved surface. Furthermore, Γ_2 and Γ_1 can be regarded as coincident due to elastic deformations, allowing either to be selected as the domain Ω_f to derive the Reynolds equation. In this study, Γ_2 is chosen such that $\Omega_f = \Gamma_2$.

Assuming that Γ_2 is represented by the parametric coordinates $(\xi_1,\ \xi_2)$, a set of covariant vectors can thus be defined as $\boldsymbol{\tau}_\alpha := \boldsymbol{x}_{2,\alpha}$

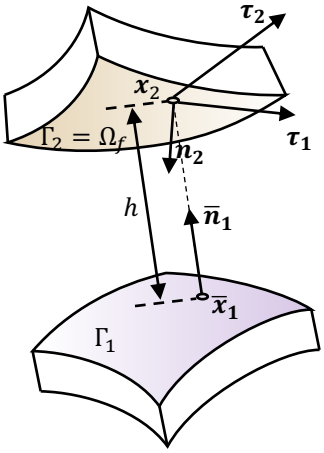

Fig. 2: Schematic illustration of deriving the Reynolds equation on the curved surface: the surface Γ_2 is chosen as the fluid domain Ω_f; the point $\boldsymbol{x}_2$ on Γ_2 is projected to $\bar{\boldsymbol{x}}_1$ on Γ_1, thereby defining the gap height h

for any point $\boldsymbol{x}_2$ on this curved surface. Herein, the subscript $(\bullet)_{,\alpha}$ denotes the partial derivative operator $\partial(\bullet)/\partial\xi_\alpha$. These tangential vectors can be transformed into a set of contravariant vectors $\boldsymbol{\tau}^\alpha$ using the metric tensor $\boldsymbol{M}$:

$$\boldsymbol{\tau}^\alpha = M^{\alpha\beta}\boldsymbol{\tau}_\beta, \quad M^{\alpha\beta} = (\boldsymbol{M})_{\alpha\beta} = \boldsymbol{\tau}_\alpha \cdot \boldsymbol{\tau}_\beta. \tag{1}$$

Notably, all Greek letters used in this work follow the Einstein notation. Utilizing these auxiliary vectors, the gradient operator $\boldsymbol{\nabla}_f(\bullet)$ and the divergence operator $\boldsymbol{\nabla}_f \cdot (\bullet)$ on the curved surface Ω_f can be defined as

$$\boldsymbol{\nabla}_f(\bullet) = (\bullet)_{,\alpha} \otimes \boldsymbol{\tau}^\alpha, \quad \boldsymbol{\nabla}_f \cdot (\bullet) = (\bullet)_{,\alpha} \cdot \boldsymbol{\tau}^\alpha. \tag{2}$$

Given the primary objective of this work is to establish an IGA framework for hip prostheses, the transient flow is not considered here. Drawing upon the derivations from Temizer and Stupkiewicz (2016), the Reynolds equation on Ω_f under the steady condition is expressed as

$$\boldsymbol{\nabla}_f \cdot (\bar{\rho}\bar{\boldsymbol{u}}h) = 0, \tag{3}$$

$$\bar{\boldsymbol{u}} = \boldsymbol{u}_m - \frac{h^2}{12\eta}\boldsymbol{\nabla}_f p. \tag{4}$$

It consists of two parts, where Equation (3) represents the mass conservation equation. Herein, $\bar{\rho}$ and $\bar{\boldsymbol{u}}$ denote the average density and average flow velocity across the film thickness, respectively. The definition of $\bar{\boldsymbol{u}}$ is provided in Equation (4), which is essentially a simplified momentum conservation equation based on the assumptions of the Reynolds equation. $\boldsymbol{u}_m = (\boldsymbol{u}_1 + \boldsymbol{u}_2)/2$ signifies the average velocity of the two surfaces, p is the fluid pressure, and η is the realistic viscosity of the synovial fluid ($\eta = 0.0025\,\mathrm{Pa}\cdot\mathrm{s}$, as derived from Meng et al. (2015)).
In Equations (3) and (4), h represents the gap height between the two surfaces, which can be determined with the aid of the Closest Point Procedure (CPP) from computational contact mechanics (for more details refer to Wriggers (2006)). Specifically, for any point $\boldsymbol{x}_2$ on Γ_2, its projection point $\bar{\boldsymbol{x}}_1$ on Γ_1 is located such that the distance between these two points is minimized (see Fig. 2):

$$\bar{\boldsymbol{x}}_1 = \arg\min_{\boldsymbol{x}_1} \|\boldsymbol{x}_2 - \boldsymbol{x}_1\|. \tag{5}$$

Denoting the outward unit normal vector at point $\bar{\boldsymbol{x}}_1$ as $\bar{\boldsymbol{n}}_1$, the gap height at $\bar{\boldsymbol{x}}_2$ is then formulated as

$$h = (\boldsymbol{x}_2 - \bar{\boldsymbol{x}}_1) \cdot \bar{\boldsymbol{n}}_1. \tag{6}$$

To develop the IGA formulation for hip prostheses, it is necessary to first derive the weak form of the Reynolds equation on the curved surface. The detailed derivation process can be referred to Tong et al. (2022) and is thus not provided here. In brief, the mass conservation Equation (3) needs to be multiplied by an arbitrary test function δp and integrated over the entire fluid domain Ω_f. After performing integration by parts and considering $\delta p = 0$ on $\partial\Omega_f$ due to the Dirichlet boundary condition ($p = 0\,\mathrm{Pa}$), the weak form of the Reynolds equation is presented as

$$\int_{\Omega_f} \frac{\bar{\rho}h^3}{12\eta}\,\boldsymbol{\nabla}_f\delta p \cdot \boldsymbol{\nabla}_f p\,\mathrm{d}\Omega - \int_{\Omega_f} \boldsymbol{\nabla}_f\delta p \cdot (\bar{\rho}\boldsymbol{u}_m h) = 0. \tag{7}$$

The void fraction r is introduced in this work to incorporate the cavitation phenomenon. It represents the volume fraction of cavitation bubbles within the fluid film. Assuming the synovial fluid is incompressible with a density of ρ_0 leads to $\bar{\rho} = \rho_0(1 - r)$. Since the pressure in cavitation regions is constant (generally set to 0 Pa), p and r satisfy the following complementarity condition:

$$p \geq 0, \quad r \geq 0, \quad pr = 0, \tag{8}$$

also referred to as JFO boundary condition (see Bhushan (2013)). Tong et al. (2022) employ the augmented Lagrangian method (AL) to transform this inequality constraint into solving the following weak formulation:

$$\int_{\Omega_f} \delta r C_r = 0, \tag{9}$$

$$C_r = \begin{cases} -p, & -r + \epsilon p \leq 0 \ \text{(cavitated)} \\ -\dfrac{1}{\epsilon} r, & -r + \epsilon p > 0 \ \text{(full film)} \end{cases}, \tag{10}$$

where the AL parameter $\hat{r} = -r + \epsilon p$ is utilized to differentiate between the cavitation region and the full-film region, and ϵ is defined as a positive penalty parameter. It can be chosen arbitrarily since its primary function is to adjust the convergence speed. The advantage of this AL formulation lies in its C^1-continuity, enabling its solution via the Newton-Raphson method.
By substituting $\bar{\rho} = \rho_0(1 - r)$ into Equation (7) and considering that $r\boldsymbol{\nabla}_f p = \mathbf{0}$ over the entire fluid domain, the weak formulation can be derived as

$$\int_{\Omega_f} \frac{h^3}{12\eta} \boldsymbol{\nabla}_f \delta p \cdot \boldsymbol{\nabla}_f p \, \mathrm{d}\Omega - \int_{\Omega_f} \boldsymbol{\nabla}_f \delta p \cdot (\boldsymbol{u}_m h) \, \mathrm{d}\Omega + \int_{\Omega_f} \boldsymbol{\nabla}_f \delta p \cdot (r\boldsymbol{u}_m h) \, \mathrm{d}\Omega = 0. \tag{11}$$

It is noteworthy that a divergence term $\boldsymbol{\nabla}_f \cdot (r\boldsymbol{u}_m h)$ appears in the original Reynolds equation (3) with the introduction of the new variable r, corresponding to the third integral term in the weak formulation (11). Since the modified Reynolds equation lacks a diffusion term for r, it can be considered a convection-dominated equation. Stabilization techniques similar to the upwind scheme, such as the Streamline upwind Petrov–Galerkin (SUPG) method outlined in Brooks and Hughes (1982), are required to eliminate non-physical oscillations in the solutions. The stabilized weak formulation of the Reynolds equation can be expressed as

$$\begin{aligned} &\int_{\Omega_f} \frac{h^3}{12\eta} \boldsymbol{\nabla}_f \delta p \cdot \boldsymbol{\nabla}_f p \, \mathrm{d}\Omega - \int_{\Omega_f} \boldsymbol{\nabla}_f \delta p \cdot (\boldsymbol{u}_m h) \, \mathrm{d}\Omega + \int_{\Omega_f} \boldsymbol{\nabla}_f \delta p \cdot (r\boldsymbol{u}_m h) \, \mathrm{d}\Omega \\ &- \int_{\Omega_f} (\gamma \boldsymbol{u}_m \cdot \boldsymbol{\nabla}_f \delta p) \, \boldsymbol{\nabla}_f \cdot (r\boldsymbol{u}_m h) \, \mathrm{d}\Omega = 0, \end{aligned} \tag{12}$$

where γ is a stabilization parameter depending on the flow velocity and element size (for more details see Brooks and Hughes (1982) and Tong et al. (2022)).
As for the elastic acetabular cup, its deformation can be described by the classical linear momentum balance equation. In this work, the acetabular cup is assumed to undergo small deformations. The reference configuration and the deformed configuration are thus considered nearly identical. Denoting the reference configuration of the acetabular cup as Ω_2, its deformation is then governed by

$$\boldsymbol{\nabla} \cdot \boldsymbol{\sigma} = 0, \tag{13}$$

where $\boldsymbol{\sigma}$ is the Cauchy stress tensor, and $\boldsymbol{\nabla} \cdot (\bullet)$ is the divergence operator in Ω_2.
The weak form of Equation (13) can be obtained following the established procedures in conventional FEA (analogous to deriving the virtual work):

$$\int_{\Omega_2} \boldsymbol{\nabla}\delta\boldsymbol{u} : \boldsymbol{\sigma} \, \mathrm{d}\Omega - \int_{\Gamma_2} \delta\boldsymbol{u} \cdot \boldsymbol{t} \, \mathrm{d}\Gamma = 0. \tag{14}$$

Herein, $\delta\boldsymbol{u}$ is the test function and satisfies $\delta\boldsymbol{u} = \mathbf{0}$ on the fixed outer surface of the acetabular cup. In addition, $\boldsymbol{t}$ signifies the traction arising from the fluid-structure interaction on Γ_2. Given that the fluid pressure acts perpendicularly on the solid surface, $\boldsymbol{t}$ is expressed as

$$\boldsymbol{t} = -p\boldsymbol{n}_2, \tag{15}$$

where $\boldsymbol{n}_2$ denotes the outward unit normal vector on Γ_2. Substituting Equation (15) into Equation (14) yields

$$\int_{\Omega_2} \boldsymbol{\nabla}\delta\boldsymbol{u} : \boldsymbol{\sigma} \, \mathrm{d}\Omega + \int_{\Gamma_2} \delta\boldsymbol{u} \cdot p\boldsymbol{n}_2 \, \mathrm{d}\Gamma = 0. \tag{16}$$

Ultimately, the weak formulations (9), (12), and (16) collectively describe the fluid-structure interaction within the hip prosthesis. They can be iteratively solved using the Newton-Raphson method after discretization.

3 NURBS-based Isogeometric Analysis

NURBS is renowned for its capability to exactly describe spherical surfaces and various conic surfaces, making it particularly suitable for hip prosthesis modeling. The specific settings for constructing the acetabular cup in Fig. 1 using NURBS can be found in Piegl and Tiller (1995). In essence, this process involves creating a semicircular ring on the xy-plane and then rotating it around the y-axis for half a revolution (or considering it as the trajectory of a semicircle) to obtain the final three-dimensional geometry. Notably, NURBS requires only 32 control points (similar to the concept of nodes in conventional FEA) to accurately construct this complex shape (as shown in Fig. 3). The three knot parameters (u, v, and w) of this NURBS geometry correspond to the

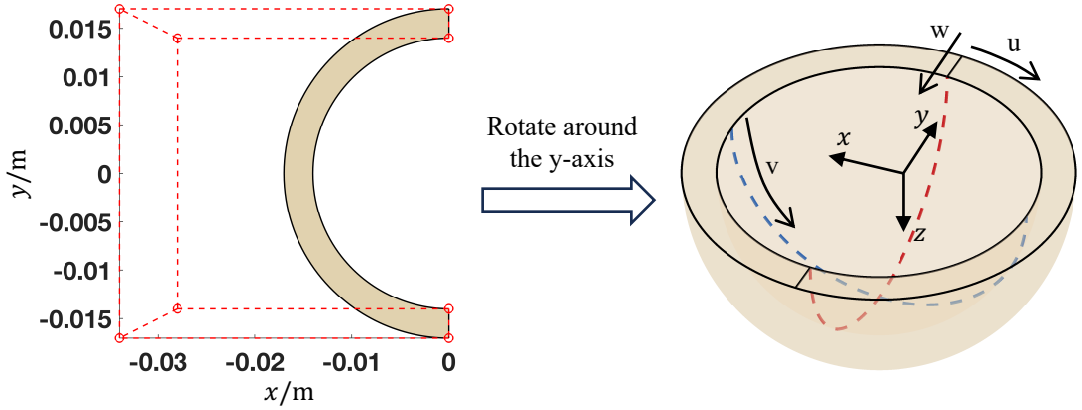

Fig. 3: Construction of the acetabular cup using NURBS: a semicircular ring on the xy-plane can be built using $4 \times 2 = 8$ control points, corresponding to 1 element (left); rotating it around the y-axis yields the acetabular cup with $4 \times 2 \times 4 = 32$ control points, corresponding to 1 element (right).

longitudinal, latitudinal and radial directions of the acetabular cup, respectively. Moreover, since the elements of NURBS geometry are directly defined in its knot parameter space, the corresponding mesh is automatically generated upon the completion of the geometric construction (for instance, the initial geometry possesses 1 element as shown in Fig. 3), eliminating the need for an additional meshing process as in FEA.

Certainly, the NURBS mesh in Fig. 3 cannot be directly used for computing complex physical fields. Thanks to the k-refinement technique in NURBS, it is possible to elevate the mesh's polynomial order to any desired one or to enhance the element resolution without altering the NURBS geometry. For instance, Fig. 4 demonstrates the refinement of the initial mesh from merely one element to 4000 elements (corresponding to 6877 control points). Given that this work defines the fluid domain directly on the inner surface of the acetabular cup, it comprises thus 400 elements (corresponding to 529 control points).

Within a NURBS mesh, each control point is associated with a NURBS basis function, denoted as R_A $(A = 1, \ldots, n_{cp})$ Consequently, the unknown field variables p, r, $\boldsymbol{u}$ and their variations derived in the previous section can be interpolated using these basis functions as

$$p = \sum_{A=1}^{n_{cp}} R_A p_A, \qquad r = \sum_{A=1}^{n_{cp}} R_A r_A, \qquad \boldsymbol{u} = \sum_{A=1}^{n_{cp}} R_A \boldsymbol{u}_A, \tag{17}$$

$$\delta p = \sum_{A=1}^{n_{cp}} R_A \delta p_A, \qquad \delta r = \sum_{A=1}^{n_{cp}} R_A \delta r_A, \qquad \delta \boldsymbol{u} = \sum_{A=1}^{n_{cp}} R_A \delta \boldsymbol{u}_A, \tag{18}$$

where p_A, r_A, and $\boldsymbol{u}_A$ represent the pressure, void fraction, and displacement at control point A, respectively, and n_{cp} denotes the total number of control points. The weak formulations (9), (12), and (16) can be discretized by substituting the interpolated variables in Equations (17) and (18). The unknown parameters at each control point are then solved using the Newton-Raphson method. The specific derivation process can be referred to Tong et al. (2022) and is thus not provided here.

4 Results

This section presents results for the scenario shown in Fig. 1, obtained from the IGA-based hip prosthesis model. The eccentricity of the femoral head (e_x, e_y, e_z) is set as $(0, 0, 0.95c)$, resulting in a minimal undeformed gap height of $0.05c = 500\,\text{nm}$.

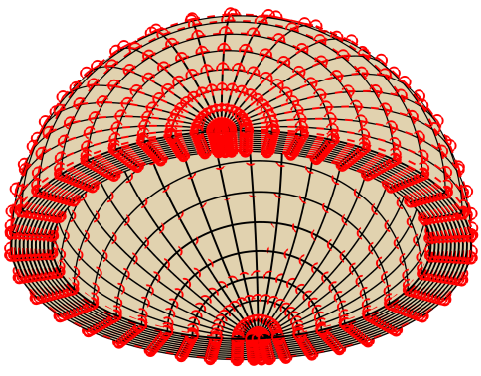

Fig. 4: Refining the initial NURBS mesh to $20 \times 10 \times 20 = 4000$ elements, corresponding to $23 \times 13 \times 23 = 6877$ control points; the inner surface of the acetabular cup is chosen as the fluid domain, it possesses $20 \times 20 = 400$ elements, corresponding to $23 \times 23 = 529$ control points

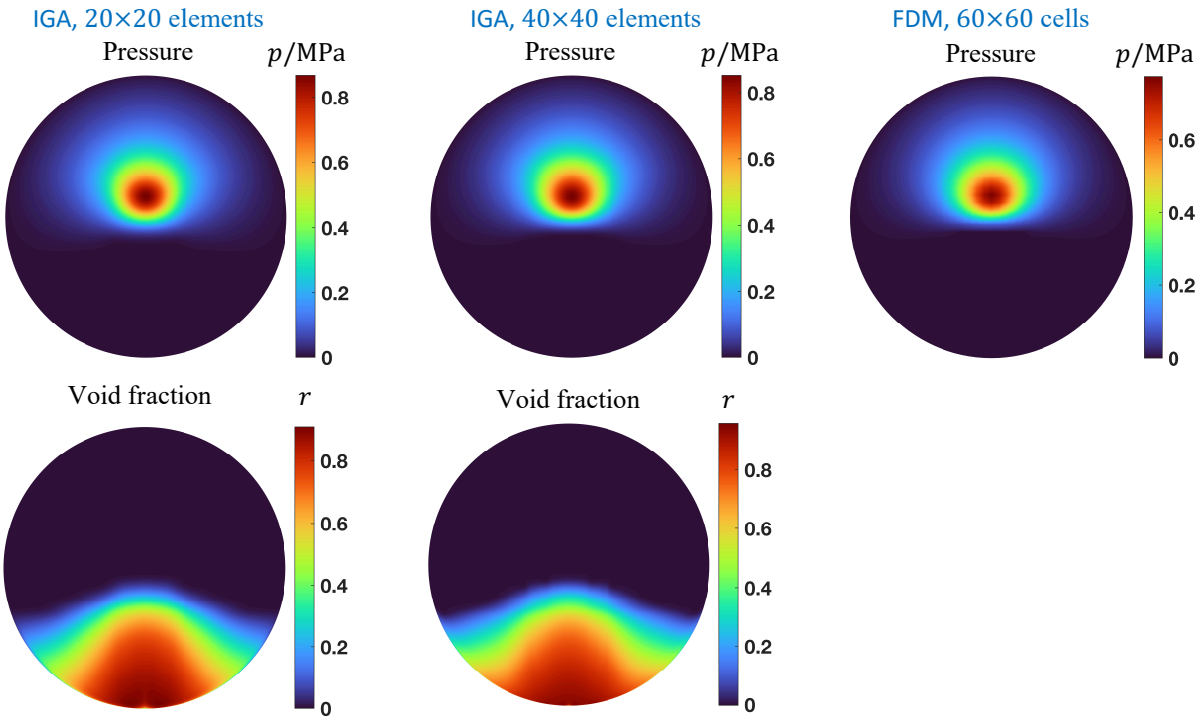

Fig. 5: Results not considering deformation for the eccentricity of (0, 0, 0.95c), obtained from the IGA-based model and the FDM-based model: pressure distribution p (first row) and void fraction r (second row)

For comparison, calculations will also be conducted using Jin and Dowson (1999)'s FDM-based model. Notably, It employs the Swift-Stieber cavitation condition and is thus limited to computing pressure distributions without addressing void fraction distributions. To closely align the computational scenarios of both models, the IGA-based model in this section will use the fully flooded condition, assuming that the fluid domain's boundaries are always sufficiently lubricated, thus $r = 0$ on $\partial\Omega_f$.

To evaluate the sensitivity of the IGA model to meshing resolution, this section employs not only the mesh depicted in Fig. 4 (with 20×20 elements for the fluid domain) but also refines the mesh for both the inner and outer surfaces of the acetabular cup, including the fluid domain, to 40×40 elements. In the FDM model, the fluid domain is divided into 60×60 cells within a spherical coordinate system.

Fig. 5 displays results that do not consider elastic deformation. The outcomes obtained with both coarse and fine NURBS meshes in the IGA model are almost identical, indicating that even with a coarse mesh (with 20×20 elements for the fluid domain), a converged solution can be achieved. In contrast, despite utilizing the highest number of elements in the fluid domain, the pressure distribution derived from the FDM model exhibits noticeable pixelation, lacking the smoothness of the IGA model's solution. Moreover, the pressure contours calculated by the FDM model are very similar to those obtained by the IGA model, albeit slightly lower in magnitude. This discrepancy stems from the different cavitation conditions employed. The IGA model uses the mass-conserving JFO condition, which reveals a large bubble forming beneath the fluid domain, hence concentrating the lubricant above the fluid domain. In contrast, the FDM model employs the Swift-Stieber condition, which posits a zero pressure gradient at the cavitation interface.

The results considering deformations of the acetabular cup are presented in Fig. 6. The IGA model also achieves converged results using the coarse mesh. The pressure calculated by the FDM model is significantly smaller than that obtained by the IGA model. This difference arises from the equation used to calculate deformation in these two models. The FDM model employs the Boussinesq equation, based on half-space theory, which considers deformation on an infinitely long surface and is thus not suitable for curved surfaces like a sphere. However, the IGA model utilizes the momentum balance equation from continuum mechanics, enabling a more accurate description of the deformation on curved surfaces.

The impact of the surface deformation on fluid pressure is illustrated in Fig. 7, where the symmetrical longitudinal curve (the red dashed line in Fig. 3) is selected to observe the pressure distribution. The maximum deformation calculated by the IGA model is about 250 nm, which is significant compared to the minimal undeformed gap height of 500 nm. Hence, the pressure considering deformation is considerably lower than that without deformation. Furthermore, Fig. 7 also clearly demonstrates the robustness of the IGA model. High-quality results can be obtained even with the coarse NURBS mesh, converging in only 8 iterations, whereas the FDM model requires more than 2000 iterations to converge.

5 Summary and Outlook

This work develops an IGA-based numerical framework for hip prostheses, employing strong coupling to calculate both the fluid pressure and solid deformation. It also incorporates a developed cavitation formulation to account for the formation and volumetric distribution of cavitation bubbles. The Reynolds equation describing fluid flow within the framework is derived for arbitrary surfaces, hence offering excellent extensibility. The results demonstrate that the IGA-based model, even when utilizing a coarse

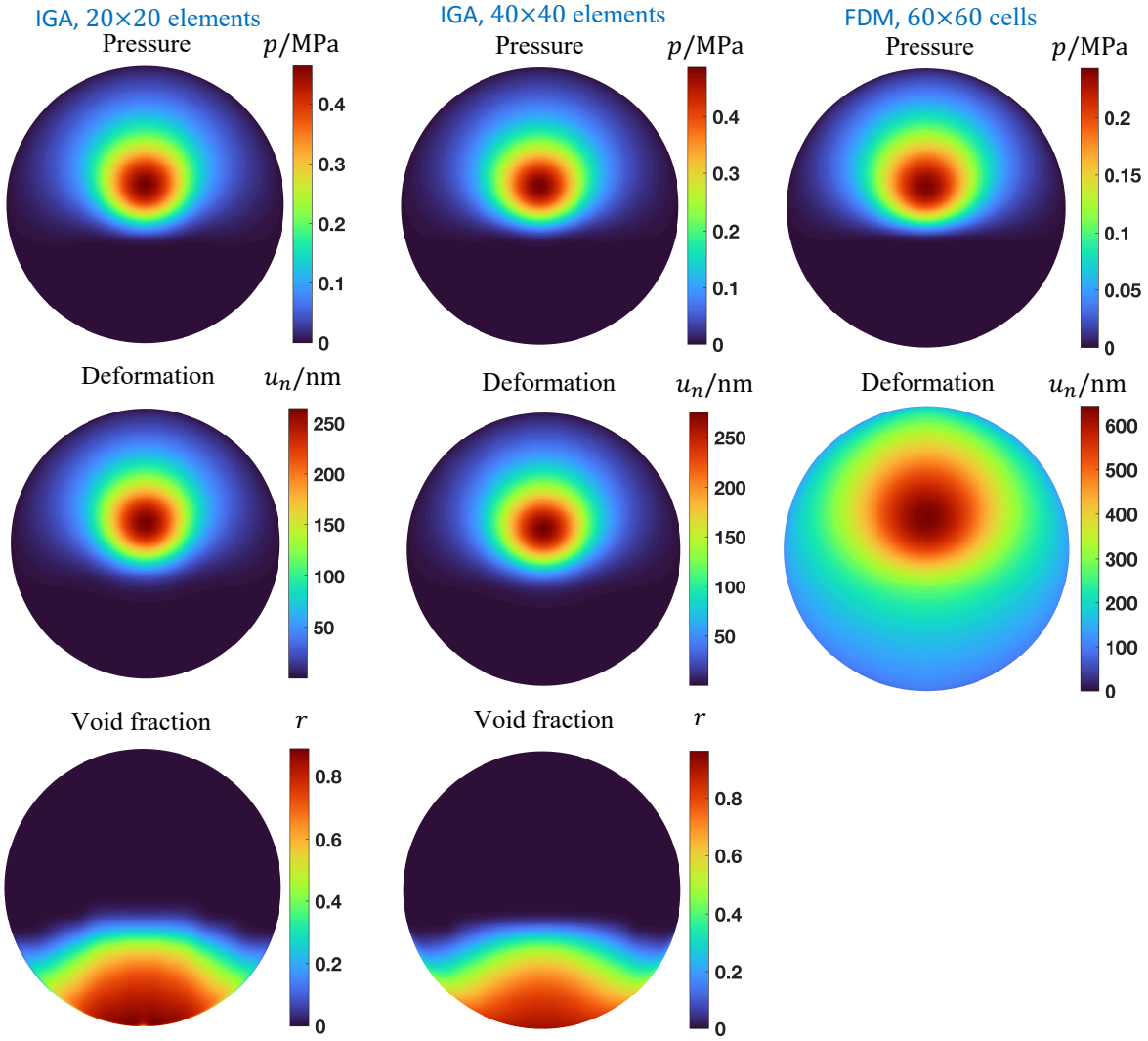

Fig. 6: Results considering deformation for the eccentricity of $(0, 0, 0.95c)$, obtained from the IGA-based model and the FDM-based model: pressure distribution p (first row), deformation in the radial direction u_n (second row) and void fraction r (third row)

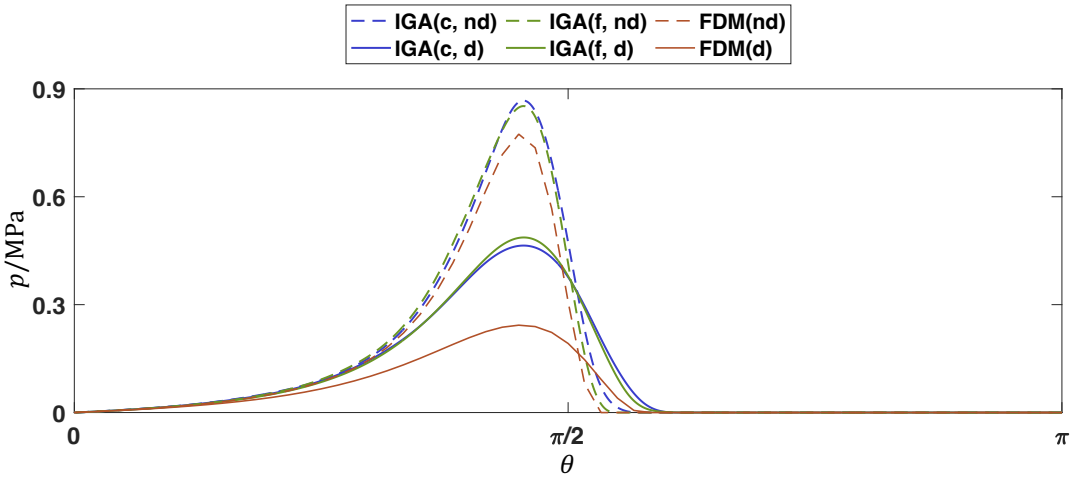

Fig. 7: Comparison of the pressure distribution along the symmetrical longitudinal curve (see the red dashed curve in Fig. 3, represented using the polar angle θ in spherical coordinates): "c" for "coarse NURBS mesh", "f" for "fine NURBS mesh", "nd" for "without deformation" and "d" for "with deformation"

NURBS mesh, efficiently delivers high-quality results within a limited number of iterations, underscoring its superior performance in elastohydrodynamic lubrication modeling. Future work could consider the nonlinear large deformation of solids or even couple this framework with frictional contact formulations (see Tong et al. (2021)) to further investigate the lubrication mechanisms in hip prostheses.

Acknowledgment and Funding Information

This work was supported by the German Research Foundation (project number 390252106).

References

E. Askari and M.S. Andersen. A modification on velocity terms of reynolds equation in a spherical coordinate system. *Tribology International*, 131:15–23, 2019. ISSN 0301-679X. doi: https://doi.org/10.1016/j.triboint.2018.10.019. URL https://www.sciencedirect.com/science/article/pii/S0301679X18305000.

Bharat Bhushan. *Fluid Film Lubrication*, chapter 8, pages 399–500. John Wiley and Sons, Ltd, 2013. ISBN 9781118403259. doi: https://doi.org/10.1002/9781118403259.ch8. URL https://onlinelibrary.wiley.com/doi/abs/10.1002/9781118403259.ch8.

Alexander N. Brooks and Thomas J.R. Hughes. Streamline upwind/petrov-galerkin formulations for convection dominated flows with particular emphasis on the incompressible navier-stokes equations. *Computer Methods in Applied Mechanics and Engineering*, 32(1):199–259, 1982. ISSN 0045-7825. doi: https://doi.org/10.1016/0045-7825(82)90071-8. URL https://www.sciencedirect.com/science/article/pii/0045782582900718.

Jonathan T Evans, Jonathan P Evans, Robert W Walker, Ashley W Blom, Michael R Whitehouse, and Adrian Sayers. How long does a hip replacement last? a systematic review and meta-analysis of case series and national registry reports with more than 15 years of follow-up. *The Lancet*, 393(10172):647–654, 2019. ISSN 0140-6736. doi: https://doi.org/10.1016/S0140-6736(18)31665-9. URL https://www.sciencedirect.com/science/article/pii/S0140673618316659.

T.J.R. Hughes, J.A. Cottrell, and Y. Bazilevs. Isogeometric analysis: Cad, finite elements, nurbs, exact geometry and mesh refinement. *Computer Methods in Applied Mechanics and Engineering*, 194(39):4135–4195, 2005. ISSN 0045-7825. doi: https://doi.org/10.1016/j.cma.2004.10.008. URL https://www.sciencedirect.com/science/article/pii/S0045782504005171.

M Jagatia and Z M Jin. Elastohydrodynamic lubrication analysis of metal-on-metal hip prostheses under steady state entraining motion. *Proceedings of the Institution of Mechanical Engineers, Part H: Journal of Engineering in Medicine*, 215(6):531–541, June 2001. ISSN 2041-3033. doi: 10.1243/0954411011536136. URL http://dx.doi.org/10.1243/0954411011536136.

Z. M. Jin and D Dowson. A full numerical analysis of hydrodynamic lubrication in artificial hip joint replacements constructed from hard materials. *Proceedings of the Institution of Mechanical Engineers, Part C: Journal of Mechanical Engineering Science*, 213(4):355–370, April 1999. ISSN 2041-2983. doi: 10.1243/0954406991522310. URL http://dx.doi.org/10.1243/0954406991522310.

Qingen Meng, Jing Wang, Peiran Yang, Zhongmin Jin, and John Fisher. The lubrication performance of the ceramic-on-ceramic hip implant under starved conditions. *Journal of the Mechanical Behavior of Biomedical Materials*, 50:70–76, 2015. ISSN 1751-6161. doi: https://doi.org/10.1016/j.jmbbm.2015.06.001. URL https://www.sciencedirect.com/science/article/pii/S1751616115001939.

M. Müller, A. Völpel, and G.-P. Ostermeyer. On the influence of fluid dynamics and elastic deformations on pressure buildup in partially filled gaps. *Tribology International*, 105:345–359, 2017. ISSN 0301-679X. doi: https://doi.org/10.1016/j.triboint.2016.08.039. URL https://www.sciencedirect.com/science/article/pii/S0301679X16302924.

Michael Müller, Lukas Stahl, and Georg-Peter Ostermeyer. Experimental studies of lubricant flow and friction in partially filled gaps. *Lubricants*, 6(4):110, December 2018. ISSN 2075-4442. doi: 10.3390/lubricants6040110. URL http://dx.doi.org/10.3390/lubricants6040110.

Les Piegl and Wayne Tiller. *The NURBS Book*. Springer Berlin Heidelberg, 1995. ISBN 9783642973857. doi: 10.1007/978-3-642-97385-7. URL http://dx.doi.org/10.1007/978-3-642-97385-7.

Valentin L. Popov. *Contact Mechanics and Friction*. Springer Berlin Heidelberg, 2010. ISBN 9783642108037. doi: 10.1007/978-3-642-10803-7. URL http://dx.doi.org/10.1007/978-3-642-10803-7.

İ. Temizer and S. Stupkiewicz. Formulation of the reynolds equation on a time-dependent lubrication surface. *Proceedings of the Royal Society A: Mathematical, Physical and Engineering Sciences*, 472(2187):20160032, March 2016. ISSN 1471-2946. doi: 10.1098/rspa.2016.0032. URL http://dx.doi.org/10.1098/rspa.2016.0032.

Yan Tong, Michael Müller, and Georg-Peter Ostermeyer. Investigations on the dynamic influence of the contact angle on frictional sliding processes between rough surfaces using nurbs and mortar-based augmented lagrangian method. *Tribology International*, 158:106889, 2021. ISSN 0301-679X. doi: https://doi.org/10.1016/j.triboint.2021.106889. URL https://www.sciencedirect.com/science/article/pii/S0301679X21000372.

Yan Tong, Michael Müller, and Georg-Peter Ostermeyer. A mortar-based cavitation formulation using nurbs-based isogeometric analysis. *Computer Methods in Applied Mechanics and Engineering*, 398:115263, 2022. ISSN 0045-7825. doi: https://doi.org/10.1016/j.cma.2022.115263. URL https://www.sciencedirect.com/science/article/pii/S0045782522003905.

P.S. Walker and B.L. Gold. The tribology (friction, lubrication and wear) of all-metal artificial hip joints. *Wear*, 17(4):285–299, 1971. ISSN 0043-1648. doi: https://doi.org/10.1016/0043-1648(71)90032-9. URL https://www.sciencedirect.com/science/article/pii/0043164871900329.

F. C. Wang and Z. M. Jin. Elastohydrodynamic Lubrication Modeling of Artificial Hip Joints Under Steady-State Conditions. *Journal of Tribology*, 127(4):729–739, 03 2005. ISSN 0742-4787. doi: 10.1115/1.1924460. URL https://doi.org/10.1115/1.1924460.

Peter Wriggers. *Computational Contact Mechanics*. Springer Berlin Heidelberg, 2006. ISBN 9783540326090. doi: 10.1007/978-3-540-32609-0. URL http://dx.doi.org/10.1007/978-3-540-32609-0.